Regenerative Therapy 14 (2020) 19–31

Contents lists available at ScienceDirect

Regenerative Therapy

journal homepage: http://www.elsevier.com/locate/reth

Original Article

Stepwise strategy for generating osteoblasts from human pluripotent stem cells under fully defined xeno-free conditions with small-molecule inducers

Denise Zujur [a], Kosuke Kanke [b], Shoko Onodera [c], Shoichiro Tani [b], Jenny Lai [a], Toshifumi Azuma [c], Xiaonan Xin [d], Alexander C. Lichtler [d], David W. Rowe [d], Taku Saito [b], Sakae Tanaka [b], Hideki Masaki [e], Hiromitsu Nakauchi [e, f], Ung-il Chung [a, g], Hironori Hojo [a, g], Shinsuke Ohba [a, g, *, 1]

[a] *Department of Bioengineering, Graduate School of Engineering, The University of Tokyo, Tokyo, Japan*
[b] *Department of Sensory and Motor System Medicine, Graduate School of Medicine, The University of Tokyo, Tokyo, Japan*
[c] *Department of Biochemistry, Tokyo Dental College, Tokyo, Japan*
[d] *Department of Reconstructive Sciences, University of Connecticut Health Center, Farmington, CT, USA*
[e] *Center for Stem Cell Biology and Regenerative Medicine, Institute of Medical Science, The University of Tokyo, Tokyo, Japan*
[f] *Institute for Stem Cell Biology and Regenerative Medicine, Stanford University School of Medicine, Stanford, CA, USA*
[g] *Center for Disease Biology and Integrative Medicine, Graduate School of Medicine, The University of Tokyo, Tokyo, Japan*

ARTICLE INFO

Article history:
Received 5 September 2019
Received in revised form
20 November 2019
Accepted 24 December 2019

Keywords:
Mesoderm
Wnt
Hedgehog
Helioxanthin
Three-dimensional culture

ABSTRACT

Clinically relevant human induced pluripotent stem cell (hiPSC) derivatives require efficient protocols to differentiate hiPSCs into specific lineages. Here we developed a fully defined xeno-free strategy to direct hiPSCs toward osteoblasts within 21 days. The strategy successfully achieved the osteogenic induction of four independently derived hiPSC lines by a sequential use of combinations of small-molecule inducers. The induction first generated mesodermal cells, which subsequently recapitulated the developmental expression pattern of major osteoblast genes and proteins. Importantly, Col2.3-Cherry hiPSCs subjected to this strategy strongly expressed the cherry fluorescence that has been observed in bone-forming osteoblasts *in vivo*. Moreover, the protocol combined with a three-dimensional (3D) scaffold was suitable for the generation of a xeno-free 3D osteogenic system. Thus, our strategy offers a platform with significant advantages for bone biology studies and it will also contribute to clinical applications of hiPSCs to skeletal regenerative medicine.

© 2020, The Japanese Society for Regenerative Medicine. Production and hosting by Elsevier B.V. This is an open access article under the CC BY-NC-ND license (http://creativecommons.org/licenses/by-nc-nd/4.0/).

1. Introduction

Induced pluripotent stem cells (iPSCs) have emerged as a promising option for disease modeling, drug screening, and cell-based therapies. The prompt translation of iPSC technology to various tissues depends largely on the development of efficient protocols for iPSC differentiation, which must be safe and facile while producing functional cells. In particular, defined protocols directing pluripotent stem cells (PSCs) toward specific lineages are required to achieve not only clinical grade cells but also to stably reproduce tissue formation processes and disease status *in vitro*; batch-to-batch variation of undefined culture components, e.g., fetal bovine serum (FBS), possibly affects the cell fate decision and the outcome of the culture.

At present, several strategies to generate clinically relevant human iPSC (hiPSC) derivatives under xeno-free conditions have been described. Induced lineages include retinal cells [1,2], hepatocytes [3], cardiomyocytes [4], endothelial cells [5], neuronal cells [6], and more. In the skeletal field, several strategies have been reported to direct human PSCs (hPSCs) including hiPSCs toward

---

[*] Corresponding author. Department of Cell Biology, Institute of Biomedical Science, Nagasaki University, 1-7-1 Sakamoto, Nagasaki, Japan. Fax: +81 95 819 7633.
E-mail address: shinohba-tky@umin.ac.jp (S. Ohba).

Peer review under responsibility of the Japanese Society for Regenerative Medicine.

[1] Present address: Department of Cell Biology, Institute of Biomedical Science, Nagasaki University, Nagasaki, Japan

https://doi.org/10.1016/j.reth.2019.12.010
2352-3204/© 2020, The Japanese Society for Regenerative Medicine. Production and hosting by Elsevier B.V. This is an open access article under the CC BY-NC-ND license (http://creativecommons.org/licenses/by-nc-nd/4.0/).

osteoblasts, which are responsible for bone formation and maintenance [7–11]. Although they successfully induce osteoblastic cells from hPSCs, there may still be a room for improvement in terms of definiteness of culture components and simplification of procedures.

Osteoblast differentiation is a sequential process regulated by local and systemic signaling molecules. A number of signaling pathways have been shown to play roles during osteoblast specification and differentiation, such as hedgehog (Hh) [12–15], Wnt [16–19], bone morphogenetic proteins (BMP) [20], and fibroblast growth factor (FGF) [21]. However, the complex interactions and the stage-specific actions of those pathways present a challenge to the design of effective protocols for directing hPSCs into osteoblasts. In addition, the contribution of those pathways to osteoblast development was revealed mainly by mouse genetic studies, which may not accurately reflect human skeletal development, raising a concern about species-related discrepancies between protocols intended for osteoblast differentiation.

Based on the accumulated knowledge about key signaling pathways for osteoblast development, we developed a small molecule-mediated induction protocol for directing PSCs toward osteoblasts [22]. The protocol enabled the successful osteoblast differentiation of mouse PSCs (mPSCs) via mesoderm formation under defined conditions by sequential treatment with combinations of four small-molecule inducers [22]. However, the induction ability of the protocol in hiPSCs was limited. In the present study, we optimized the osteogenic molecular pathways to differentiate hiPSCs into osteoblasts under fully defined xeno-free conditions, and we propose an optimized strategy for generating osteoblasts from hiPSCs.

2. Materials and methods

2.1. Adaptation and maintenance of hiPSCs under xeno-free conditions

Four independently derived hiPSC lines (hiPSC-1, hiPSC-2, hiPSC-3, and hiPSC-4) were used in this study. Human neonatal fibroblast-derived iPSCs (hiPSC-1) were established from commercially available human neonatal dermal fibroblasts (Lonza, Basel, Switzerland) by transducing the human *POU5F1*, *SOX2*, *KLF4*, and *MYC* genes [22]. 201B7 (hiPSC-2; HPS0063) [23] and Nips-B2 (hiPSC-3; HPS0223) [24] were obtained from RIKEN BioResource Research Center (Tsukuba, Japan). To establish the Col2.3-Cherry hiPSC line (hiPSC-4), human skin fibroblasts were initially reprogrammed with *POU5F1*, *SOX2*, *KLF4*, and *MYC* using Sendai virus vectors (provided by DNAVEC/ID Pharma, Tsukuba, Japan). Site-specific integration of the Col2.3-RFPcherry reporter into the "safe harbor" *AAVS1* locus was then achieved as described previously [25], except that the CRIPSR/Cas approach was used to target the *AAVS1* locus instead of zinc finger nucleases. The hiPSCs were maintained on mouse embryonic fibroblasts (MEFs) in DMEM/F12 supplemented with 20% (vol/vol) KnockOut Serum Replacement (KSR) (#10828-028; Invitrogen, Carlsbad, CA, USA), 0.1 mM MEM non-essential amino acids (#11140-050; Gibco, Grand Island, NY, USA), 0.1 mM 2-mercaptoethanol (#21985-023; Gibco), and 5 ng/mL recombinant human FGF2 (#064-04541; Wako, Osaka, Japan). For the osteoblast induction, the hiPSCs were first adapted and maintained in a commercially available xeno-free culture system (E8/VTN) using Essential 8™ medium (E8; Thermo Fisher Scientific, Waltham, MA, USA) and recombinant human vitronectin (VTN) (#A14700; Gibco)-coated dishes (5 μg/mL). Typically, hiPSCs were well adapted after 6–10 passages. For the dissociation of the cells, we used 0.5 mM EDTA (#15575-020; Gibco).

2.2. Differentiation of hiPSCs into osteoblasts under serum-free conditions

hiPSCs adapted to E8/VTN were maintained on six-well plates up to 70% confluency (day 0). Mesoderm differentiation was achieved by 3-day treatment (from day 0 to day 3) with two small-molecules: CHIR99021 (20 μM, #039-20831; Wako) and cyclopamine (5 μM, #BML-GR334; Enzo Life Sciences, New York, NY, USA) in the basal differentiation medium (BM) consisting of DMEM/F12 with HEPES and L-glutamine (#11330-032; Gibco), 0.1 mM MEM non-essential amino acids (#11140-050; Gibco), 0.1 mM 2-mercaptoethanol (#21985-023; Gibco), B-27 Serum-Free Supplement (#17504-044; Gibco), ITS+1 Liquid Media Supplement (#I2521; Sigma–Aldrich, St. Louis, MO, USA), and 1% penicillin-streptomycin solution (#P4458; Sigma–Aldrich). The medium was changed every day. As a comparison, mesoderm differentiation in hiPSC-1 and hiPSC-2 was also induced by 3-day culture in STEMdiff™ Mesoderm Induction Medium (#05220; Stemcell Technologies, Grenoble, France). Following the mesoderm induction, the osteogenic program was initiated on day 3 with 1 μM SAG (#566660; Calbiochem, Darmstadt, Germany) and 1 μM TH (a helioxanthin derivative, 4-(4-Methoxyphenyl)thieno [2,3-*b*:5,4-*c*′]dipyridine-2-carboxamide: #M3085; Tokyo Chemical Industry Co., Ltd., Tokyo, Japan) [22,26] in the osteogenic (OG) medium, which was the BM supplemented with 50 μg/mL ascorbic acid phosphate (AsAP) (#A4034; Sigma–Aldrich), 10 mM β-glycerophosphate (β-GP) (#G9422; Sigma–Aldrich), 0.1 μM dexamethasone (Dex) (#41-18861; Wako), and 200 ng/mL human recombinant FGF2 (#064-04541; Wako). On day 4, the cells were dissociated using Accutase (#AT104; Innovative Cell Technologies, San Diego, CA, USA) and passed to VTN-coated 12-well plates (2.5–3 × 10^5 cells/well). The medium was changed every day. Beginning on day 10, the hiPSC-derived osteoprogenitor cells were differentiated into osteoblasts by the 4-day treatment with 8 μM CHIR and 1 μM TH in the OG medium. Osteoblast maturation was subsequently achieved by culturing the cells for an additional 7 days (from day 14 to day 21) in the OG medium without any inducers. The medium was changed every day throughout the culture.

2.3. Differentiation of hiPSCs into osteoblasts under xeno-free conditions

hiPSCs adapted to E8/VTN were maintained on six-well plates up to 70% confluency (day 0). Mesoderm differentiation was achieved by the 3-day treatment with CHIR (15 μM) and Cyc (5 μM) in the xeno-free BM. The xeno-free conditions of the BM were achieved by substituting B-27 Serum-Free Supplement with B-27 Xeno-Free Supplement (#A1486701; Gibco), and ITS+1 Liquid Media Supplement with ITS Liquid Media Supplement (#I3146-5 ML; Sigma–Aldrich) in the BM. The other components were the same as those used in the BM. On day 3, the osteogenic program was initiated by 7-day treatment with 1 μM SAG and 1 μM TH in the xeno-free osteogenic medium (xeno-free OG medium), which was the xeno-free BM supplemented with 50 μg/mL AsAP, 10 mM β-GP, 0.1 μM Dex, and 100 ng/mL human recombinant FGF2. On day 4, the cells were dissociated using Accutase and passed to VTN-coated 12-well plates (2.5–3 × 10^5 cells/well). Beginning on day 10, the cells were differentiated into osteoblasts by the 2-day treatment with 4.5 μM CHIR and 1 μM TH in the xeno-free OG medium. Osteoblast

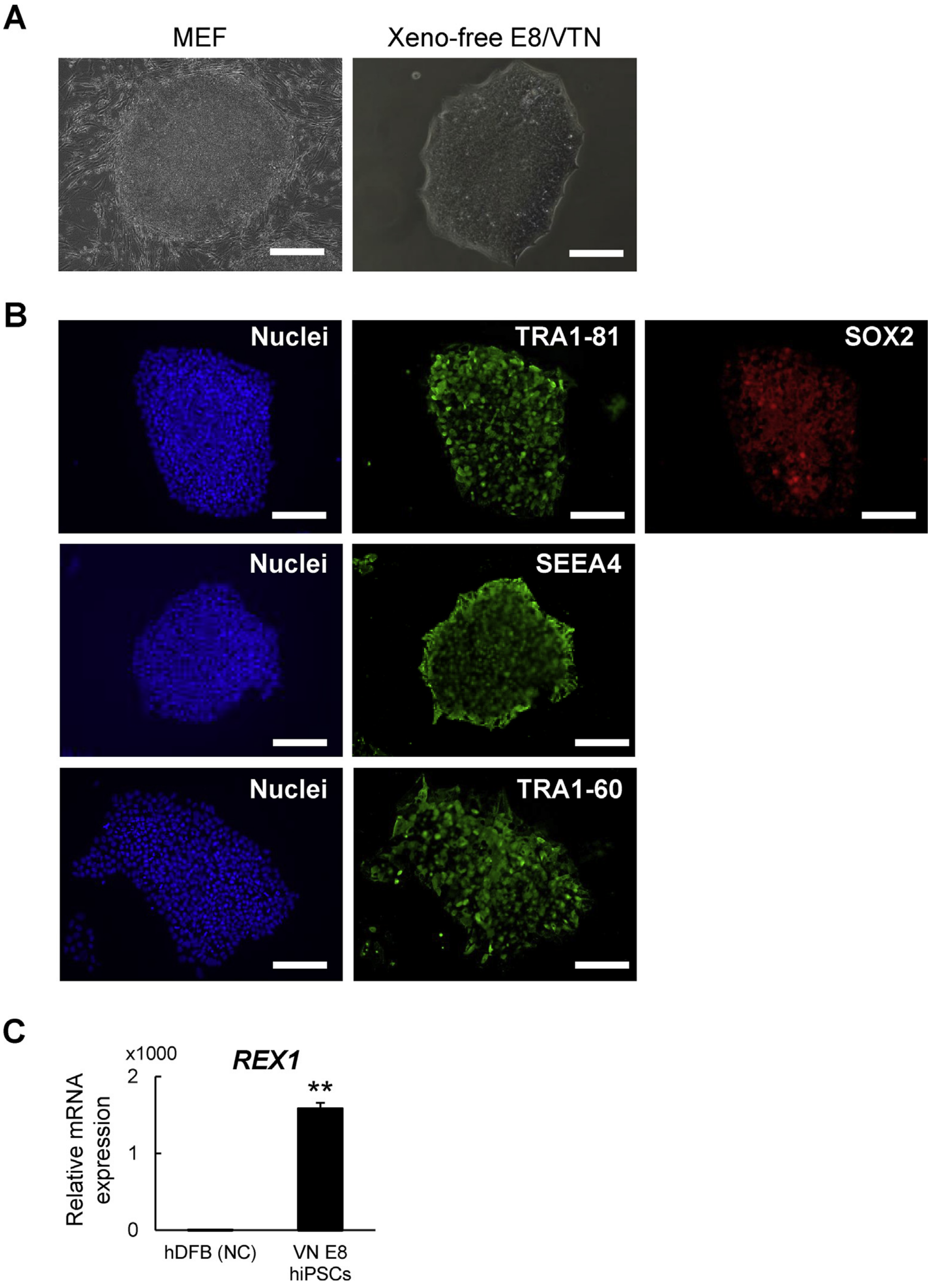

Fig. 1. Characterization of hiPSCs maintained under the xeno-free condition. (**A**) Colony morphology in hiPSC-1 maintained on MEFs (*left*) or under feeder-free and xeno-free conditions (*right*). Scale bars: 200 μm. (**B**) Immunostaining for pluripotency markers (TRA1-81, SOX2, SEEA4, and TRA1-60) in hiPSC-1 maintained under the xeno-free conditions with DAPI staining of nuclei. Scale bars: 200 μm. (**C**) The mRNA expression of *REX1* by RT-qPCR analysis in hiPSC-1 maintained under the xeno-free conditions and human dermal fibroblasts (hDFBs, negative control). Data are the means ± SD from three independent experiments. $^{**}P < 0.01$ vs. negative control.

maturation was subsequently achieved by culturing the cells for an additional 9 days (from day 12 to day 21) in the xeno-free OG medium without any inducers. The culture medium was changed every day.

2.4. Differentiation of hiPSCs into osteoblasts in 2D and 3D cultures under xeno-free conditions

hiPSC-1 was maintained in the E8/VTN system and differentiated into osteoblasts according to the xeno-free strategy described above with the following modifications. After mesoderm induction (day 4), 2.5×10^5 cells dissociated from a well were sub-cultured under 2D and 3D conditions. Temperature-responsive 12-well plates (#174899; Thermo Fisher Scientific) were used for the 2D culture and porous scaffolds were used for the 3D culture. The scaffolds were fabricated from a commercially available human type I collagen-based recombinant peptide (Cellnest™; Fujifilm, Tokyo, Japan) and were shaped upon our request as follows: discs (dia. 4 mm, height 1 mm) with pores ranging from 200 μm to 400 μm.

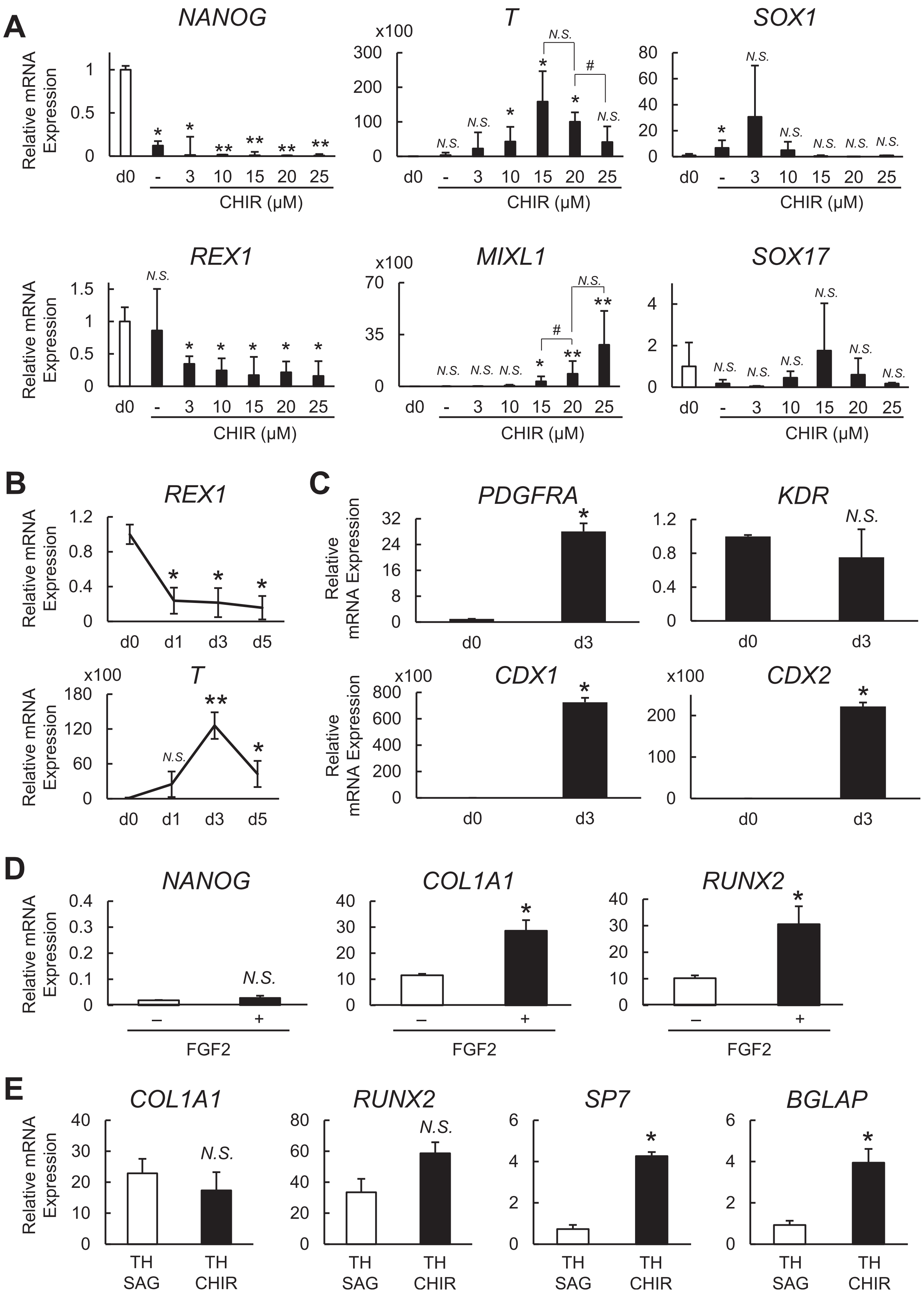
A
NANOG
T
SOX1
REX1
MIXL1
SOX17
Relative mRNA Expression
x100
N.S.
#
*
**
d0
-
3
10
15
20
25
CHIR (μM)
B
REX1
T
d1
d3
d5
C
PDGFRA
KDR
CDX1
CDX2
D
NANOG
COL1A1
RUNX2
FGF2
–
+
E
COL1A1
RUNX2
SP7
BGLAP
TH SAG
TH CHIR

For detailed experimental procedures, see Supplementary information.

3. Results

3.1. Optimization of the mesoderm induction under serum-free conditions

We initially adapted hiPSCs to Essential 8 medium on vitronectin (VTN)-coated plates, referred to as "the E8/VTN system" hereafter. The E8/VTN system is a fully defined xeno-free culture system [27]. The adaptation was successfully achieved within 10 passages, as shown by the typical morphology of the hiPSC colonies (Fig. 1A) with strong expression of pluripotency markers (Fig. 1 B, C).

To develop a protocol for differentiating hiPSCs into the osteoblast lineage under defined xeno-free conditions, we set out to follow the small molecule-based stepwise differentiation strategy that we developed [22], and to optimize each step for hiPSCs. The strategy consists of (1) the mesoderm induction of PSCs, (2) osteoblast induction from the iPSC-derived mesodermal cells, and (3) osteoblast maturation [22]. In that strategy, the activation of canonical Wnt signaling with 30 μM CHIR99021 (CHIR) and the suppression of Hh signaling with 5 μM cyclopamine (Cyc) allowed us to obtain mesodermal cells from hiPSCs within 5 days [22]. However, the strategy requires the use of plates coated with Matrigel, which is not a fully defined reagent [28], to maintain the cell viability. In the present study, we therefore examined whether treatment with a lower concentration of CHIR in combination with 5 μM Cyc and a shorter period of treatment would improve the cell survival and induce the mesoderm differentiation of hiPSCs on VTN-coated plates.

We observed that relative to day 0, the CHIR treatment downregulated the pluripotency-related genes Nanog homeobox (*NANOG*) and ZFP42 zinc finger protein (*ZFP42*; also known as *REX1*) at all concentration tested (Fig. 2A). The expressions of the mesoderm-related markers T-box transcription factor T (*TBXT*; also known as *T* or *Brachyury*) and Mix paired-like homeobox (*MIXL1*) were higher at both 15 μM and 20 μM CHIR than at lower concentrations. However, the *MIXL1* expression was significantly higher in the cells treated with 20 μM compared to those with 15 μM CHIR (Fig. 2A). The cells treated with 25 μM CHIR in turn showed a decreased expression of *T* and a comparable expression of *MIXL1* to 20 μM. We also examined SRY-box transcription factor 1 (*SOX1*) and SRY-box transcription factor 17 (*SOX17*), which are ectoderm and endoderm marker genes, respectively. *SOX1* was not upregulated at CHIR concentrations >10 μM, and *SOX17* was not significantly altered under any of the tested conditions (Fig. 2A). Therefore, we chose 20 μM CHIR and 5 μM Cyc for the mesoderm induction. Regarding the period of treatment, we found that a 3-day treatment was optimal, as the expression of *T* was higher on day 3 (d3) than on day 1 (d1) or day 5 (d5), whereas no significant difference was found in *REX1* between those periods (Fig. 2B).

We further evaluated the expression of other mesoderm-related genes in hiPSC cultured by the optimized mesoderm induction strategy (Fig. 2C). Platelet derived growth factor receptor alpha (*PDGFRA*), caudal type homeobox 1 (*CDX1*), and caudal type homeobox 2 (*CDX2*) were upregulated, whereas kinase insert domain receptor (*KDR*), a proposed marker for the mesodermal subpopulation committed to hematoendothelial and cardiovascular rather than mesenchymal lineages [29,30], was not significantly altered compared to day 0. $KDR^{low}/PDGFR\text{-}\alpha^{high}$ populations were reported to display paraxial mesodermal phenotypes, which specifically exhibit osteogenic, chondrogenic, and myogenic differentiation potential *in vitro* [31]. These data suggest that our optimized strategy is able to generate hiPSC-derived mesodermal cells, and that it likely proceeds at least partly via a process similar to the paraxial mesoderm specification.

3.2. Optimization of the osteoblast differentiation under serum-free conditions

The specification of the hiPSC-derived mesodermal cells into osteoblast precursors following the mesoderm induction was achieved by the treatment with 1 μM concentrations of two small molecules, the Smoothened agonist SAG and the helioxanthin derivative TH, for the next 7 days (from day 4 to day 10) in the osteogenic medium (see the Experimental Procedures) as done in our previous strategy [22]. Since FGF2 has been positively implicated in human osteoblastic population [32,33], we examined the combinatorial effect of FGF2 and SAG + TH. On day 10, the FGF2-treated cells showed significantly higher expression of early osteoblast marker genes (*RUNX2* and *COL1A1*) compared to the untreated cells, whereas *NANOG* expression was unaltered between the two conditions (Fig. 2D).

Canonical Wnt signaling is necessary for the transition of *Runx2*-positive osteoblast precursors to *Bglap*-positive osteoblasts through *Sp7*-positive precursors [16–19]. In addition, Hh signaling was shown to be dispensable for the terminal differentiation of osteoblasts [19], and sustained Hh signaling was actually found to suppress the osteoblast number and activity [34]. Based on this knowledge, we then evaluated whether the CHIR-mediated stimulation of canonical Wnt signaling and the cancellation of Hh activation following the 7-day early osteoblast differentiation phase further induced the expression of markers for early and late stage osteoblasts. The treatment with 8 μM CHIR in the presence of TH from day 10 to day 14 induced upregulations of *SP7* and *BGLAP* expression compared to the treatment with SAG + TH on day 14, whereas no significant difference was found in *RUNX2* or *COL1A1* expression (Fig. 2E). This result suggests that the hiPSC-derived osteoblast precursors are further differentiated into osteoblasts by the subsequent CHIR treatment.

Fig. 2. Optimization of the protocol for mesoderm induction and osteoblast differentiation in hiPSCs. (**A**) The mRNA expression of pluripotency (*NANOG* and *REX1*), mesoderm (*T* and *MIXL1*), ectoderm (*SOX1*), and endoderm (*SOX17*) markers determined by RT-qPCR analysis in hiPSC-1 treated for 3 days with 5 μM cyclopamine (Cyc) and CHIR at different concentrations. Data are the means ± SD from four independent experiments. $^*P < 0.05$ and $^{**}P < 0.01$ vs. all others. $^{\#}P < 0.05$ as indicated. (**B**) The mRNA expression of *REX1* and *T* determined by RT-qPCR analysis in hiPSC-1 before (d0) and after the treatment with 5 μM Cyc and 20 μM CHIR for 1 day (d1), 3 days (d3), and 5 days (d5). Data are the means ± SD from three independent experiments. $^*P < 0.05$ and $^{**}P < 0.01$ vs. d0. (**C**) The mRNA expression of mesoderm-related genes (*PDGFRA*, *KDR*, *CDX1*, and *CDX2*) determined by RT-qPCR analysis in hiPSC-1 before (d0) and after treatment with 5 μM Cyc and 20 μM CHIR for 3 days (d3). Data are the means ± SD from four independent experiments. $^*P < 0.01$ vs. d0. (**D**) The mRNA expression of pluripotency (*NANOG*) and osteoblast markers (*COL1A1* and *RUNX2*) on day 10 determined by RT-qPCR analysis in hiPSC-1-derived mesodermal cells treated with TH and SAG in the presence (+) or absence (−) of FGF2 for 7 days (from day 4 to day 10). Data analyzed relative to day 0 are shown as the means ± SD from three independent experiments. $^*P < 0.05$ vs. FGF2 (−) group. (**E**) The mRNA expression of osteoblast markers on day 14 determined by RT-qPCR analysis in hiPSC1-derived osteogenic cells treated with TH and SAG or TH and CHIR for 4 days (from day 10 to day 14) in the presence of FGF2. Data analyzed relative to day 0 are shown as the means ± SD from three independent experiments. $^*P < 0.05$ vs. TH + SAG group.

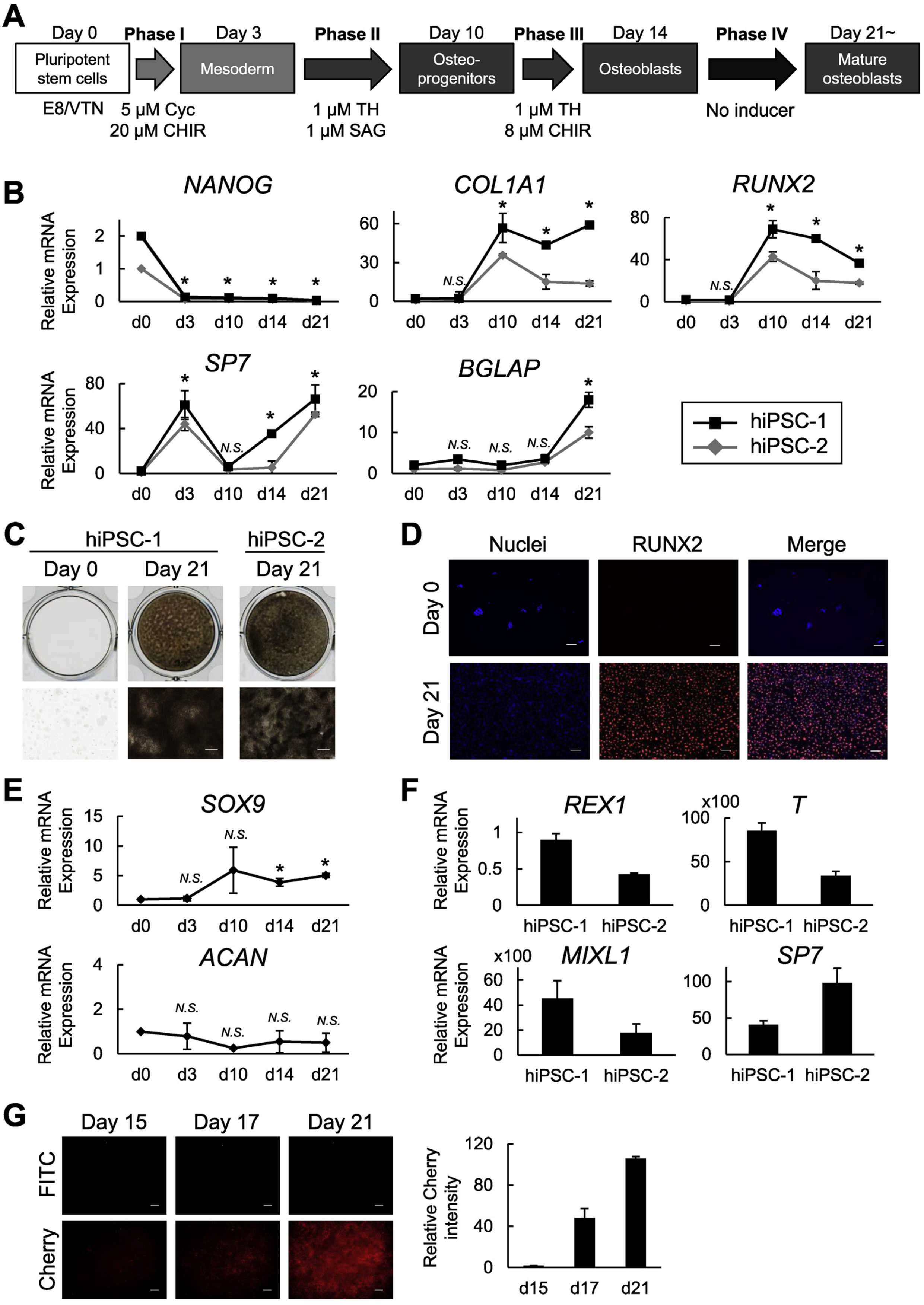
A
Day 0
Pluripotent stem cells
E8/VTN
Phase I
5 μM Cyc
20 μM CHIR
Day 3
Mesoderm
Phase II
1 μM TH
1 μM SAG
Day 10
Osteo-progenitors
Phase III
1 μM TH
8 μM CHIR
Day 14
Osteoblasts
Phase IV
No inducer
Day 21~
Mature osteoblasts
B
NANOG
COL1A1
RUNX2
SP7
BGLAP
Relative mRNA Expression
d0
d3
d10
d14
d21
N.S.
*
hiPSC-1
hiPSC-2
C
hiPSC-1
hiPSC-2
Day 0
Day 21
D
Nuclei
RUNX2
Merge
Day 0
Day 21
E
SOX9
ACAN
F
REX1
T
MIXL1
SP7
x100
G
Day 15
Day 17
Day 21
FITC
Cherry
Relative Cherry intensity
d15
d17
d21

3.3. Characterization of the optimized protocol for the osteoblast differentiation of hiPSCs

As described above, we optimized the protocol for differentiating hiPSCs into osteoblast (Fig. 3A). The protocol includes three phases that we optimized here: a 3-day mesoderm induction (phase I), a 7-day osteoblast specification (phase II), and a 4-day osteoblast differentiation (phase III), followed by an osteoblast maturation for 7 days or more (phase IV) that was included in our previous strategy. The additional culture without inducers was proposed to allow further maturation of the osteogenic cell population derived from hiPSCs [22].

Fig. 3B shows the time course of the osteoblast-related marker expression in two independently derived hiPSC lines, hiPSC-1 and hiPSC-2 (see Materials and methods), cultured under the protocol. Both lines showed similar gene expression patterns. *RUNX2* was upregulated at the end of the osteoblast specification phase (day 10), and decreased as the differentiation advanced. *COL1A1* was also upregulated on day 10, and the expression at later points trended down to varying degrees between the two lines. *SP7* was upregulated during the mesoderm induction phase (from day 0 to day 3; Phase I) and downregulated during the osteoblast specification phase (Phase II); it was then upregulated again during the osteoblast differentiation phase (Phase III) and finally reached a peak at Phase IV. *BGLAP* was progressively upregulated during the osteoblast maturation phase (from day 14 to day 21; Phase IV). In addition, matrix calcification was largely observed at the Phase IV (on day 21) as was indicated by von Kossa staining (Fig. 3C). The immunohistochemical examination of hiPSC-1 revealed the nuclear localization of RUNX2 in most of the induced cells at the Phase IV (86 ± 6% on day 21) (Fig. 3D). We also evaluated the time course of the expressions of *SOX9* and *ACAN* in hiPSC-1, which are makers for osteo-chondroprogenitors and committed chondrocytes, respectively [35]. *SOX9* was slightly upregulated after the mesodermal induction, with an increase of fivefold compared to day 0 or day 3, whereas *ACAN* did not show upregulation at any time point (Fig. 3E). These data suggest that our strategy can reproduce the expression pattern of major osteogenic markers in osteoblast development but not those in chondrocyte development. One exception was *SP7*; our strategy induced a transient upregulation of *SP7* at the mesoderm induction stage (Phase I), although *SP7* has not been implicated in the early mesodermal population. This phenomenon is unlikely to be specific to our strategy, since hiPSC-1 and hiPSC-2 cultured in a commercially available mesoderm induction medium for 3 days (see Materials and methods) also showed the upregulations of *SP7* and mesoderm markers with a downregulation of the pluripotency marker *REX1* (Fig. 3F).

To further examine the *in vivo* relevance of the hiPSC-derived osteoblastic population generated by the present strategy, we cultured Col2.3-Cherry hiPSCs (see Materials and methods) carrying a transgene in which the red fluorescent protein (RFP) Cherry was driven by a 2.3-kb rat *Col1a1* promoter fragment, and we monitored the Cherry-derived florescence signal throughout the culture. Cherry expression driven by the activation of the fragment can be used as a bona-fide indicator of "*in vivo*-functional osteoblasts" for the following three reasons. First, the green fluorescent protein (GFP) signal driven by the Col1a1 promoter fragment was observed exclusively in osteoblasts and osteocytes in Col2.3-GFP transgenic mouse lines [36]. Second, when a Col2.3-GFP human embryonic stem cell (hESC)-derived mesenchymal population or Col2.3-GFP human bone marrow mesenchymal stem cells (MSCs) were transplanted to a critical-sized mouse calvarial bone defect, GFP-positive cells contributed to orthotopic bone formation *in vivo* [25,37]. Third, the Col2.3-GFP transgene has successfully enabled the monitoring of osteoblast differentiation in mouse ESCs [22,38,39].

In the present experiments, Cherry fluorescence started to appear at the onset of phase IV (osteoblast maturation phase, day 15). It then gradually increased during the culture and reached high levels throughout the Phase IV (Fig. 3G). Col2.3-Cherry iPSCs further enabled us to assess differentiation efficiency of the present strategy by flow cytometry. The flow cytometry data from biological duplicate supported our findings so far in a reproducible manner (Fig. 4). The Phase IV population contained a larger percentage of RUNX2-positive early osteoblastic cells and Cherry-positive osteoblastic cells than the non-induced population (Runx2$^+$ cells: 71.2% and 53.6% in the Phase IV vs. 20.4% and 19.2% in the non-induced; Cherry$^+$ cells: 17.3% and 19.4% in the Phase IV vs. 4.5% and 3.6% in the non-induced). Consistent with the increase in the differentiated population, cells positive for the pluripotency marker TRA1-81 were substantially reduced in the Phase IV population compared to the non-induced one. These findings suggest that the present strategy achieves the lineage specification of hiPSCs into mesodermal cells, the subsequent differentiation of the hiPSC-derived mesodermal cells into osteoblasts, and eventually the generation of mature osteoblasts, which are potentially functional *in vivo*.

3.4. Optimization of the present strategy under xeno-free conditions

Considering the potential applications of the present strategy to cell-based therapies, we next attempted to expand the present strategy to xeno-free conditions. These conditions were achieved by substituting the supplements with their xeno-free equivalents in the basal medium (BM), and by slightly modifying the concentration and period of treatment of small-molecule inducers to improve the cell viability that was decreased by the substitution of supplements. Since the expressions of *T* and *MIXL1* were higher at both 15 μM and 20 μM CHIR (Fig. 2A), we decreased the CHIR concentration during the Phase I from 20 μM to 15 μM. We also reduced the period of the CHIR treatment during the Phase III from 4 days to 2 days and decreased the CHIR concentration from 8 μM to 4.5 μM. Fig. 5A shows the modified osteoblast differentiation protocol for the fully defined xeno-free conditions.

The 3-day mesoderm induction with 15 μM CHIR and 5 μM Cyc under the xeno-free conditions strongly induced the expression of mesoderm marker genes (*T* and *MIXL1*) and the downregulation of *REX1* in three hiPSC lines (Fig. 5B). When hiPSC-derived mesodermal cells were then differentiated into osteoblasts (phases II–IV) under the xeno-free conditions, the gene expression profiles

Fig. 3. Characterization of hiPSC-derived cells induced by the present strategy under serum-free conditions. (**A**) A schematic of the four-phase strategy for osteoblast differentiation of hiPSCs using small molecule inducers under serum-free conditions. (**B**) Time course of the mRNA expression determined by an RT-qPCR analysis in two independently derived hiPSC lines (hiPSC-1 and hiPSC-2) cultured using the present strategy for osteoblast differentiation. Data are the means ± SD from four independent experiments. $^*P < 0.05$ at the indicated time points (d3, d10, d14, and d21) vs. day 0 in both hiPSC-1 and hiPSC-2. (**C**) Representative pictures of von Kossa staining in the osteogenic culture of the two hiPSC lines. Scale bars: 200 μm. (**D**) Immunostaining for RUNX2 in the osteogenic culture of hiPSC-1 on days 0 (negative control) and 21 with DAPI staining of nuclei. Scale bars: 50 μm. (**E**) Time course of the mRNA expression of *SOX9* and *ACAN* determined by RT-qPCR analysis in hiPSC-1 cultured under the serum-free strategy for osteoblast differentiation. Data are the means ± SD from four independent experiments. $^*P < 0.05$ at the indicated time points (d3, d10, d14, and d21) vs. day 0. (**F**) The mRNA expression of pluripotency (*REX1*), mesoderm (*T* and *MIXL1*), and osteoblast markers (*SP7*) determined by RT-qPCR analysis in hiPSC-1 treated with a commercially available mesoderm induction medium for 3 days (relative to day 0). Data are the means ± SD from three independent experiments. (**G**) Representative pictures of Cherry expression in Col2.3-Cherry hiPSCs (scale bars: 100 μm) and the time-line quantification of the Cherry fluorescence intensity. Data are the means ± SD from three independent experiments.

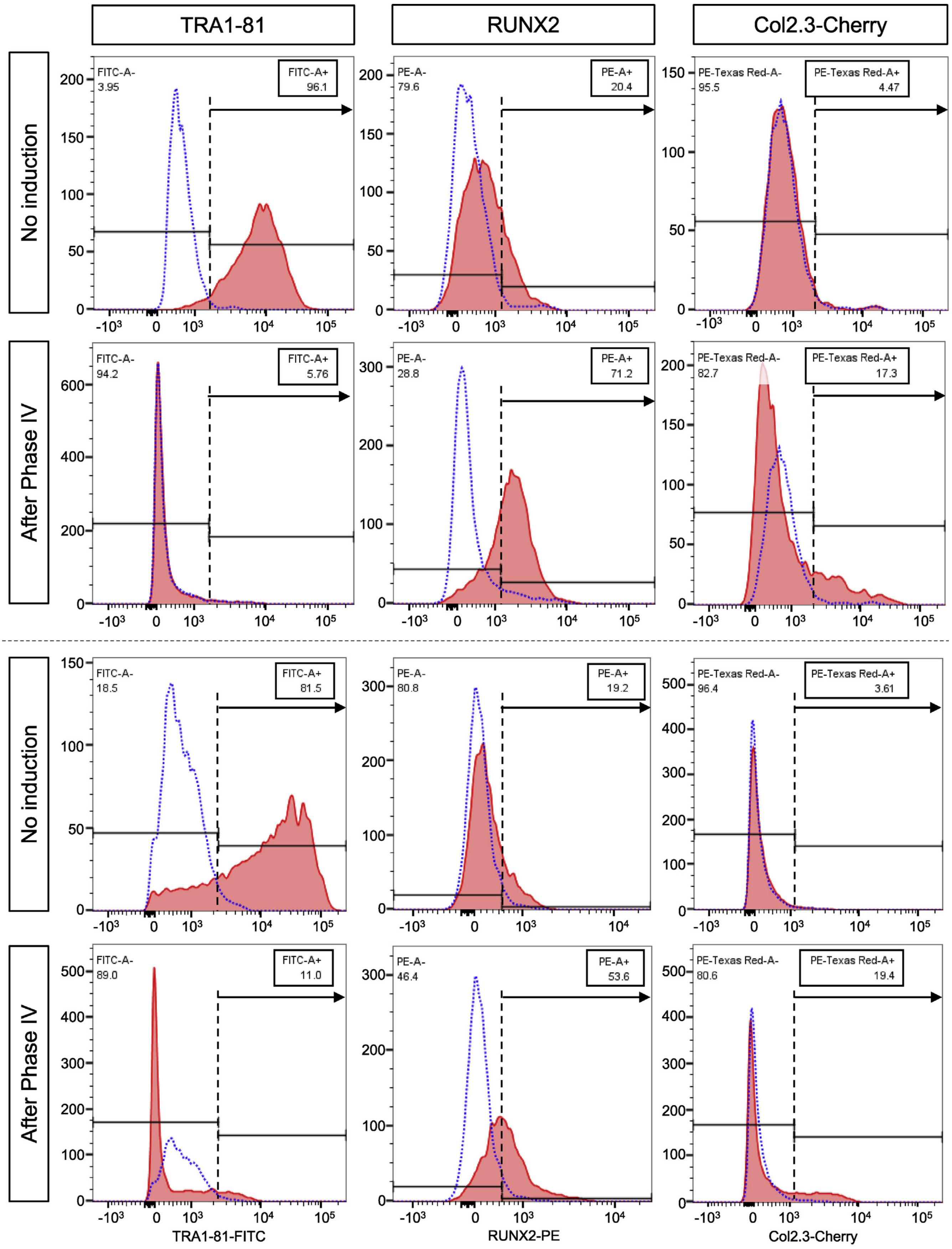
TRA1-81
RUNX2
Col2.3-Cherry
No induction
After Phase IV
No induction
After Phase IV
FITC-A-
3.95
FITC-A+
96.1
PE-A-
79.6
PE-A+
20.4
PE-Texas Red-A-
95.5
PE-Texas Red-A+
4.47
FITC-A-
94.2
FITC-A+
5.76
PE-A-
28.8
PE-A+
71.2
PE-Texas Red-A-
82.7
PE-Texas Red-A+
17.3
FITC-A-
18.5
FITC-A+
81.5
PE-A-
80.8
PE-A+
19.2
PE-Texas Red-A-
96.4
PE-Texas Red-A+
3.61
FITC-A-
89.0
FITC-A+
11.0
PE-A-
46.4
PE-A+
53.6
PE-Texas Red-A-
80.6
PE-Texas Red-A+
19.4
-10³
0
10³
10⁴
10⁵
TRA1-81-FITC
RUNX2-PE
Col2.3-Cherry

were similar to those under the serum-free conditions (compare hiPSC-1 and hiPSC-2 between Figs. 3B and 5C), and the three hiPSC lines showed strong matrix calcification on day 21 (Fig. 5D). In addition, the Col2.3-Cherry hiPSCs that were differentiated under the xeno-free conditions showed the upregulation of not only the osteoblast markers, but also osteocyte markers on day 21 (Fig. 5E), with extensive expressions of Col2.3-Cherry (Fig. 5F). Consistent with our previous findings in hiPSC-1, a slight upregulation of *SOX9*, but not *ACAN*, was detected at day 21 compared to day 0. Moreover, *NKX2.5*, a marker largely expressed in lateral plate mesoderm as well as cardiomyocytes, was not significantly upregulated. These results indicate that the improved strategy can successfully direct the osteoblast differentiation of four hiPSC lines via mesoderm formation under the fully defined xeno-free conditions.

Since three-dimensional (3D) culture systems are evolving as a convenient approach for both regenerative medicine and *in vitro* tissue models [39–41], we lastly examined whether our proposed xeno-free strategy is well-suited for a 3D culture (see Materials and methods). Mesodermal cells derived from hiPSC-1 were differentiated into osteoblasts on thermo-responsive plates (2D) or with human type I collagen-based scaffolds (3D). We compared the differentiation status of the line between the two culture conditions. The experimental design is shown in Fig. 6A.

The cells differentiated in the 3D culture showed mRNA expressions of the osteoblast-related markers (*RUNX2*, *COL1A1*, *SP7* and *BGLAP)* on day 21 that were comparable to those of the cells cultured in the 2D culture, whereas no significant difference was found in the mRNA expression of *REX1* between the two conditions (Fig. 6B). Calcification in the 2D and 3D cultures was confirmed by von Kossa staining (Fig. 6C) and the histological features were examined with H&E staining on cell sheet (2D) and scaffold (3D) sections (Fig. 6D). Although the cell distribution and morphology of the extracellular matrix (ECM) were similar between the two culture conditions, the ECM in the 3D culture exhibited a denser structure. Thus, the developed xeno-free protocol is likely to be suitable for the development of relevant osteogenic 3D cultures, and it can also be applied to the cell-sheet strategy with the thermo-responsive plate, supporting its potential advantages in hiPSC-derived osteoblast sheet-based therapies.

4. Discussion

We have established a fully defined, xeno-free, and stepwise strategy in which hiPSCs are maintained and differentiated into mature osteoblasts *in vitro*. As mentioned in the Results section, an educated guess based on developmental biology led us to test crucial regulators for osteoblast development in order to optimize each differentiation step.

The results presented here suggest that the signaling pathways that we need to manipulate for *in vitro* osteoblast differentiation are different between human and mouse iPSCs. Whereas the mesoderm induction and osteoblast specification (Phases I and II) were achieved in hiPSCs with the same set of small molecule inducers as used in mPSC differentiation, the osteoblast differentiation (Phase III) in hiPSCs required additional exogenous signaling stimulation as well as cancellation of the one signaling activated in the Phase II.

The initial treatment with CHIR and Cyc induced the differentiation of hiPSCs and mPSCs [22] into mesodermal cells. The activation of canonical Wnt signaling induces the specification of mESCs and hESCs into primitive streak (PS), a progenitor population for both the mesoderm and endoderm [42,43]. On the other hand, the inhibition of Hh signaling has been shown to prevent neuroectoderm derivatives from PSCs [44]. In our strategy, the combinatorial effect of CHIR and Cyc in hiPSCs resulted in a population that specifically expressed a wide range of paraxial mesoderm markers, whereas the key endoderm and ectoderm markers were not upregulated.

In contrast to mPSC cultures [22], the hiPSC-derived mesodermal cells showed a transient upregulation of *SP7*, which was considered to be an osteoblast marker. The mechanisms that govern *SP7* expression remain to be fully identified. Although mouse genetic studies demonstrated that *Sp7* acts genetically downstream of *Runx2* in skeletal tissues [45,46], human *SP7* was detected in several mesoderm-derived human tissues other than skeletal tissues, such as testis, heart, lung, spleen, and placenta [47]. In line with this, we observed in the present study that the *SP7* expression in the hiPSC-derived mesodermal cells was not accompanied by *RUNX2* expression, which suggests that there may be *RUNX2*-independent gene regulatory machinery for *SP7* in human mesoderm tissues.

Indeed, *Sp7* expression can be directly regulated by signaling pathways such as BMP [48] and transcription factors including Msx [48], Dlx [49], and NFκB [50]. Since our strategy used CHIR to induce the mesoderm differentiation, it is also possible that Wnt-mediated mechanisms underlie the *SP7* expression in that phase. Although further detailed analyses are required to understand the gene regulatory mechanisms and to gain functional insights into *SP7* regulation in human mesodermal cells, our data together with those of other studies suggest that SP7 functions may vary among species in this context.

The subsequent treatment of hiPSC-derived mesodermal cells with SAG and TH in the presence of FGF2 successfully induced the expression of early osteoblasts markers. SAG and TH exerted similar effects in mPSCs and hiPSCs; the rationale for using SAG and TH in this phase was supported by our previous findings [22,51] and mouse genetic studies [12,13]. The effects of FGF2 on osteogenic cultures of human versus mouse cells are a matter of controversy; FGF2 has been shown to have roles in both the differentiation and proliferation of osteoblasts in both mouse and human cells [32,33,52–54]. Since FGF2 is also known to play a key role in the pluripotency maintenance of hESCs and hiPSCs [55], but not in that of their mouse counterparts, we infer that hiPSC-derived mesodermal cells undergoing osteogenic specification may rely more on the FGF signal than mesodermal cells derived from mPSCs (at least under our culture conditions), possibly by regulating the proliferation of the progenitor pools or by directing the population toward the osteoblast lineage.

Flow cytometry and immunostaining revealed that 20–30% of cells in our culture expressed little or no RUNX2 at day 21. We consider two possibilities regarding the fates of the RUNX2-negative (RUNX2^{low}) cells. The first possibility is that the culture contains osteoblastic cells with different differentiation stages, each of which is characterized by different expression levels of RUNX2. During osteoblast development, RUNX2 protein is first detected in preosteoblasts; the expression increases in immature osteoblasts, but decreases in mature osteoblasts [45,56,57]. Based on this fact, RUNX2^{low} cells in our culture may reflect mature osteoblasts that weakly express RUNX2. The idea may be consistent

Fig. 4. Flow cytometric analysis on Col2.3-Cherry hiPSC-derived cells induced by the present strategy under serum-free conditions. Cells expressing TRA1-81 (left), RUNX2 (middle), or Cherry driven by the Col2.3 promoter fragment (right) were analyzed before the induction (No Induction) and after the Phase IV (After Phase IV). Data from biological duplicate are shown in upper and lower panels separated by the dotted line. Dotted and solid lines show signal from isotype controls (negative control) and specific antibodies, respectively. Y-axes indicate cell counts. Numbers in rectangular boxes indicate percentages of cells with positive signal.

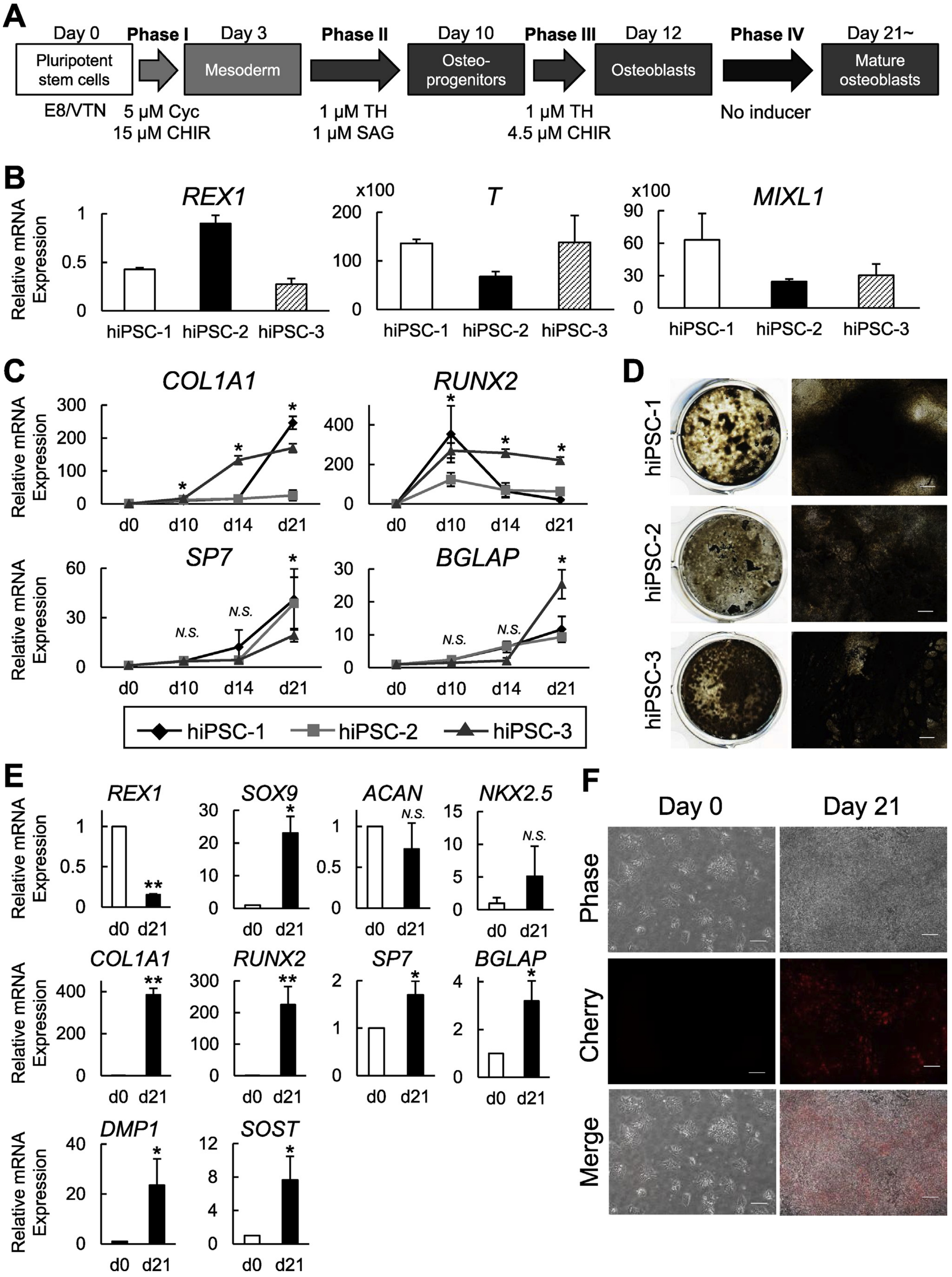
A
Day 0
Phase I
Day 3
Phase II
Day 10
Phase III
Day 12
Phase IV
Day 21~
Pluripotent stem cells
Mesoderm
Osteo-progenitors
Osteoblasts
Mature osteoblasts
E8/VTN
5 μM Cyc
15 μM CHIR
1 μM TH
1 μM SAG
1 μM TH
4.5 μM CHIR
No inducer
B
Relative mRNA Expression
REX1
1
0.5
0
hiPSC-1
hiPSC-2
hiPSC-3
x100
T
200
100
0
x100
MIXL1
90
60
30
0
C
COL1A1
300
200
100
0
d0
d10
d14
d21
*
RUNX2
400
200
SP7
60
30
N.S.
BGLAP
30
20
10
hiPSC-1
hiPSC-2
hiPSC-3
D
hiPSC-1
hiPSC-2
hiPSC-3
E
REX1
**
SOX9
ACAN
NKX2.5
15
10
5
COL1A1
RUNX2
SP7
BGLAP
DMP1
SOST
40
12
8
4
F
Day 0
Day 21
Phase
Cherry
Merge

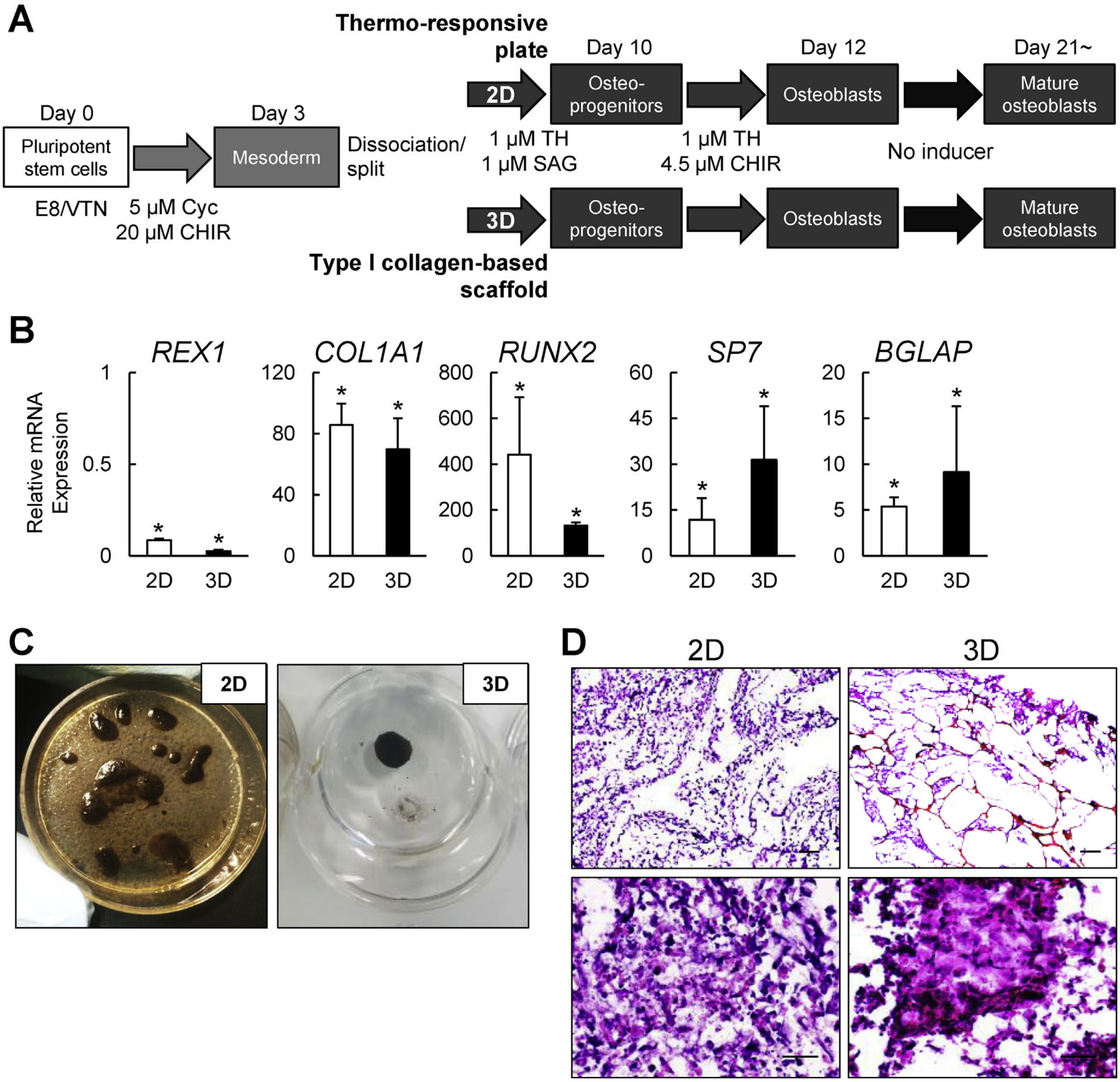

Fig. 6. Characterization of hiPSC-derived cells induced by the present strategy in the two-dimensional (2D) thermo-responsive plate culture or the three-dimensional (3D) collagen scaffold culture under the fully defined xeno-free condition. (**A**) A schematic of the osteoblast differentiation strategy in osteogenic 2D and 3D cultures under the fully defined xeno-free condition. (**B**) The mRNA expression determined by RT-qPCR analysis in hiPSC-1 differentiated in the osteogenic 2D and 3D cultures at day 21 (d21). Data are the means ± SD from three independent experiments. $^*P < 0.05$ at d21 in 2D and 3D cultures vs. d0. (**C**) Representative pictures of von Kossa staining of hiPSC-1 on day 21 in the osteogenic 2D and 3D cultures. (**D**) Representative H&E staining pictures in the 2D and 3D osteogenic cultures of hiPSC-1. Scale bars: 200 μm (upper panels) and 50 μm (lower panels).

with the time-line of *RUNX2* mRNA expression in our culture, in which *RUNX2* decreased as the differentiation advanced (day 21), and also be supported by the difference in the percentages between RUNX2-positive cells and mCherry-positive cells (Fig. 4). RUNX2 expression occurs earlier than activation of the 2.3-kb Col1a1 promoter fragment, i.e. the mCherry-positive stage in osteoblast differentiation. The promoter fragment became active in harmony with *IBSP* expression, and the activation is restricted to osteoblasts within differentiated nodules *in vitro* [58] and to periosteal mature osteoblasts and osteocytes located deep in the cortical bone *in vivo* [36]. The second possibility regarding the fates of the RUNX2-negative (RUNX2^{low}) cells is that they are not osteoblastic population; they may contain pluripotent cells remaining in the induction culture, mesodermal cells that have not yet committed to the

Fig. 5. Characterization of hiPSC-derived cells induced by the present strategy under the fully defined xeno-free conditions. (**A**) A schematic of the four-phase strategy for the osteoblast differentiation of hiPSCs under the fully defined xeno-free condition. (**B**) The mRNA expression of pluripotency (*REX1*) and mesoderm (*T* and *MIXL1*) markers determined by RT-qPCR analysis in three independently derived hiPSC lines on day 3 (relative to day 0). (**C**) Time course of the mRNA expression determined by RT-qPCR analysis in hiPSC-1, hiPSC-2, and hiPSC-3 cultured under the present xeno-free strategy for osteoblast differentiation. Data are the means ± SD from four independent experiments. $^*P < 0.05$ at the indicated time points (d10, d14, and d21) vs. day 0 in all of hiPSC-1, hiPSC-2 and hiPSC-3. (**D**) Representative pictures of von Kossa staining in the osteogenic culture of the three hiPSC lines on day 21. Scale bars: 100 μm. (**E**) The mRNA expression determined by RT-qPCR analysis in Col2.3-Cherry hiPSCs before (d0) and after the osteogenic differentiation (d21). Data are the means ± SD from three experiments. $^*P < 0.05$ at d21 vs. d0. (**F**) Representative pictures of Cherry expression in Col2.3-Cherry hiPSCs before (Day 0) and after the osteogenic differentiation (Day 21). Scale bars: 100 μm.

osteoblastic lineage, or cells that committed to other lineages. Given that heterogeneity in our system underlies both of the above possibilities, sorting RUNX2-positive cells after day 10 could potentiate our strategy.

We and others have shown that 3D culture can significantly improve the differentiation of mPSCs [39–41]. Particularly, mPSC-derived mesodermal cells showed accelerated osteogenic differentiation in the 3D culture, giving rise to functional osteoblast-osteocyte populations that were not observed in 2D cultures at the same time period of the cultures [39]. In contrast, we show in this study that molecular signature of hiPSC-derived osteoblastic population in 3D cultures are comparable to that in 2D cultures; hiPSCs were unlikely to express osteocyte markers even in the 3D culture. The timeline of events in mouse and human embryogenesis may also be reflected in the characteristics of PSCs derived from the two species, leading to the difference in their differentiation potential under certain conditions. Typically, hPSC-derived cells are difficult or need prolonged culture periods to acquire fully mature phenotypes, compared to mPSC-derived ones.

We cannot exclude the possibility that responsiveness to different external stimuli depends on an inherent capacity of each hiPSC line. Indeed, we found differences in the mRNA expression level of key osteoblast markers as well as the calcification level between different hiPSC lines. Both the differentiation potential and the response to external stimuli such as the dimensionality may vary across different lines. Substantial progress has been made in understanding of whether and how the genetic origin of donors, the type of original cells, and the reprogramming method affect the differentiation potential of iPSCs to specific lineages. For instance, epigenetic dissimilarities were found to affect the ability of hPSCs to commit to the osteogenic lineage; methylation status in *PAX7* and *TWIST1* regions was suggested to play a determining role in osteoblast development from hPSCs [59]. Extensive studies unraveling regulatory landscape on the genome during human osteoblast development are needed to further clarify this point, and our present hiPSC differentiation system potentially contributes to the studies.

One may point out two potential limitations of this study: (1) unidentified mechanisms underlying the effects of TH on osteoblast differentiation, and (2) the lack of *in vivo* evidence of the function of generated osteoblasts. We have been studying the first point and will report our findings in the near future. Regarding the second point, we need to optimize an appropriate scaffold system to maximize the *in vivo* function of *in vitro*-generated cells. Although the xeno-free human type I collagen-based scaffold allowed us to expand the osteogenic culture to a clinically relevant 3D system, it may require further optimization for *in vivo* use. We have been working on hydrogels for medical applications [60] and will report the combinatorial effect of the present hiPSC differentiation strategy and the newly developed 3D scaffold system on *in vivo* bone regeneration in the future. In addition, we obtained around 17–19% cells positive for Col2.3-Cherry in our induction culture. As mentioned in the Result section, we have shown that Col2.3-GFP hESC-derived GFP$^+$ mesenchymal population or Col2.3-GFP human MSC-derived GFP$^+$ cells were able to contribute to orthotopic bone formation *in vivo* [25,37]. Thus, the Col2.3-Cherry fluorescence in our culture at least partly supports *in vivo* osteogenic potential of the population that we generated from hiPSCs. This logic may not be in harmony with the report by Phillips et al., which showed that *in vitro* osteoblastic features of hiPSC-derived cells did not always predict their *in vivo* osteogenic potential [7]. However, given that they assessed *in vivo* potential by an ectopic bone formation model (subcutaneous transplantations of induced cells), their finding may not be the case with orthotopic bone formation models that are more clinically-relevant than ectopic bone formation models.

5. Conclusions

We have generated a robust platform to differentiate hPSCs into osteoblasts by sequentially manipulating signaling pathways involved in osteoblast specification and maturation. In contrast to the current platforms for osteoblast differentiation of hPSCs [7–11], we extensively describe the differentiation process, characterize the cells in every stage, and compare the differentiation status in multiple cell lines. This fully defined xeno-free strategy, at least to some extent, reproduces osteoblast development with confounding factors minimized, providing significant advantages for disease modeling, drug screening, and developmental studies in the skeletal field. It will also contribute to clinical applications of hPSCs to skeletal regenerative medicine.

Author contributions

D. Zujur, K. Kanke, and S. Ohba designed the project. D. Zujur, K. Kanke, S. Onodera, S. Tani, J. Lai, X. Xin, and H. Masaki performed the experiments. D. Zujur, T. Azuma, A.C. Lichtler, D.W. Rowe, T. Saito, S. Tanaka, H. Nakauchi, U. Chung, H. Hojo, and S. Ohba analyzed and interpreted the data. D. Zujur, U. Chung, H. Hojo, and S. Ohba wrote the manuscript. S. Ohba supervised the project and approved the final version of the manuscript.

Declaration of Competing Interest

The authors declare that they have no conflict of interest.

Acknowledgements

We thank Drs. Fumiko Yano, Yasuyuki Sakai, Horacio Cabral, and Takashi Ushida for the helpful discussions, and Katsue Morii, Rie Yonemoto, Akiko Nakamichi, and Nozomi Nagumo for providing technical assistance. This work utilized the core research facility of Center for Disease Biology and Integrative Medicine, The University of Tokyo, which was organized by The University of Tokyo Center for NanoBio Integration entrusted by the Ministry of Education, Culture, Sports, Science and Technology (MEXT) Japan. This work was supported by JSPS KAKENHI Grant Numbers JP26713054, JP15K15732, JP16H06312, JP17H04403, and JP18K19635; the Rising Star Award Grant from the American Society for Bone and Mineral Research (to S. Ohba) and the Japan Science and Technology Agency (JST) Center of Innovation Program (to U.C.). D.Z. and J.L. was supported by Japanese Government (MEXT) Scholarship and UTokyo Amgen Scholars Program, respectively.

Appendix A. Supplementary data

Supplementary data to this article can be found online at https://doi.org/10.1016/j.reth.2019.12.010.

References

[1] Sridhar A, Steward MM, Meyer JS. Nonxenogeneic growth and retinal differentiation of human induced pluripotent stem cells. Stem Cells Transl Med 2013;2(4):255–64.

[2] Tucker BA, Anfinson KR, Mullins RF, Stone EM, Young MJ. Use of a synthetic xeno-free culture substrate for induced pluripotent stem cell induction and retinal differentiation. Stem Cells Transl Med 2013;2(1):16–24.

[3] Farzaneh Z, Pakzad M, Vosough M, Pournasr B, Baharvand H. Differentiation of human embryonic stem cells to hepatocyte-like cells on a new developed xeno-free extracellular matrix. Histochem Cell Biol 2014;142(2):217–26.

[4] Masumoto H, Ikuno T, Takeda M, Fukushima H, Marui A, Katayama S, et al. Human iPS cell-engineered cardiac tissue sheets with cardiomyocytes and vascular cells for cardiac regeneration. Sci Rep 2014;4:6716.

[5] Bao X, Lian X, Dunn KK, Shi M, Han T, Qian T, et al. Chemically-defined albumin-free differentiation of human pluripotent stem cells to endothelial progenitor cells. Stem Cell Res 2015;15(1):122—9.
[6] Tsai Y, Cutts J, Kimura A, Varun D, Brafman DA. A chemically defined substrate for the expansion and neuronal differentiation of human pluripotent stem cell-derived neural progenitor cells. Stem Cell Res 2015;15(1):75—87.
[7] Phillips MD, Kuznetsov SA, Cherman N, Park K, Chen KG, McClendon BN, et al. Directed differentiation of human induced pluripotent stem cells toward bone and cartilage: in vitro versus in vivo assays. Stem Cells Transl Med 2014;3(7):867—78.
[8] Jeon OH, Panicker LM, Lu Q, Chae JJ, Feldman RA, Elisseeff JH. Human iPSC-derived osteoblasts and osteoclasts together promote bone regeneration in 3D biomaterials. Sci Rep 2016;6:26761.
[9] Wang P, Ma T, Guo D, Hu K, Shu Y, Xu HHK, et al. Metformin induces osteoblastic differentiation of human induced pluripotent stem cell-derived mesenchymal stem cells. J Tissue Eng Regen Med 2018;12(2):437—46.
[10] Kang H, Shih YR, Nakasaki M, Kabra H, Varghese S. Small molecule-driven direct conversion of human pluripotent stem cells into functional osteoblasts. Sci Adv 2016;2(8):e1600691.
[11] Bilousova G, Jun du H, King KB, De Langhe S, Chick WS, Torchia EC, et al. Osteoblasts derived from induced pluripotent stem cells form calcified structures in scaffolds both in vitro and in vivo. Stem Cells 2011;29(2):206—16.
[12] St-Jacques B, Hammerschmidt M, McMahon AP. Indian hedgehog signaling regulates proliferation and differentiation of chondrocytes and is essential for bone formation. Genes Dev 1999;13(16):2072—86.
[13] Long F, Chung UI, Ohba S, McMahon J, Kronenberg HM, McMahon AP. Ihh signaling is directly required for the osteoblast lineage in the endochondral skeleton. Development 2004;131(6):1309—18.
[14] Ohba S. Hedgehog signaling in endochondral ossification. J Dev Biol 2016;4(2):20.
[15] Ohba S, Kawaguchi H, Kugimiya F, Ogasawara T, Kawamura N, Saito T, et al. Patched1 haploinsufficiency increases adult bone mass and modulates Gli3 repressor activity. Dev Cell 2008;14(5):689—99.
[16] Day TF, Guo X, Garrett-Beal L, Yang Y. Wnt/beta-catenin signaling in mesenchymal progenitors controls osteoblast and chondrocyte differentiation during vertebrate skeletogenesis. Dev Cell 2005;8(5):739—50.
[17] Hill TP, Spater D, Taketo MM, Birchmeier W, Hartmann C. Canonical Wnt/beta-catenin signaling prevents osteoblasts from differentiating into chondrocytes. Dev Cell 2005;8(5):727—38.
[18] Hu H, Hilton MJ, Tu X, Yu K, Ornitz DM, Long F. Sequential roles of Hedgehog and Wnt signaling in osteoblast development. Development 2005;132(1):49—60.
[19] Rodda SJ, McMahon AP. Distinct roles for Hedgehog and canonical Wnt signaling in specification, differentiation and maintenance of osteoblast progenitors. Development 2006;133(16):3231—44.
[20] Bandyopadhyay A, Tsuji K, Cox K, Harfe BD, Rosen V, Tabin CJ. Genetic analysis of the roles of BMP2, BMP4, and BMP7 in limb patterning and skeletogenesis. PLoS Genet 2006;2(12):e216.
[21] Marie PJ. Fibroblast growth factor signaling controlling osteoblast differentiation. Gene 2003;316:23—32.
[22] Kanke K, Masaki H, Saito T, Komiyama Y, Hojo H, Nakauchi H, et al. Stepwise differentiation of pluripotent stem cells into osteoblasts using four small molecules under serum-free and feeder-free conditions. Stem Cell Rep 2014;2(6):751—60.
[23] Takahashi K, Tanabe K, Ohnuki M, Narita M, Ichisaka T, Tomoda K, et al. Induction of pluripotent stem cells from adult human fibroblasts by defined factors. Cell 2007;131(5):861—72.
[24] Ono M, Hamada Y, Horiuchi Y, Matsuo-Takasaki M, Imoto Y, Satomi K, et al. Generation of induced pluripotent stem cells from human nasal epithelial cells using a Sendai virus vector. PLoS One 2012;7(8):e42855.
[25] Xin X, Jiang X, Wang L, Stover ML, Zhan S, Huang J, et al. A site-specific integrated Col2.3GFP reporter identifies osteoblasts within mineralized tissue formed in vivo by human embryonic stem cells. Stem Cells Transl Med 2014;3(10):1125—37.
[26] Ohba S, Nakajima K, Komiyama Y, Kugimiya F, Igawa K, Itaka K, et al. A novel osteogenic helioxanthin-derivative acts in a BMP-dependent manner. Biochem Biophys Res Commun 2007;357(4):854—60.
[27] Chen G, Gulbranson DR, Hou Z, Bolin JM, Ruotti V, Probasco MD, et al. Chemically defined conditions for human iPSC derivation and culture. Nat Methods 2011;8(5):424—9.
[28] Hughes CS, Postovit LM, Lajoie GA. Matrigel: a complex protein mixture required for optimal growth of cell culture. Proteomics 2010;10(9):1886—90.
[29] Evseenko D, Zhu Y, Schenke-Layland K, Kuo J, Latour B, Ge S, et al. Mapping the first stages of mesoderm commitment during differentiation of human embryonic stem cells. Proc Natl Acad Sci U S A 2010;107(31):13742—7.
[30] Savory JG, Bouchard N, Pierre V, Rijli FM, De Repentigny Y, Kothary R, et al. Cdx2 regulation of posterior development through non-Hox targets. Development 2009;136(24):4099—110.
[31] Sakurai H, Sakaguchi Y, Shoji E, Nishino T, Maki I, Sakai H, et al. In vitro modeling of paraxial mesodermal progenitors derived from induced pluripotent stem cells. PLoS One 2012;7(10):e47078.
[32] Bosetti M, Boccafoschi F, Leigheb M, Cannas MF. Effect of different growth factors on human osteoblasts activities: a possible application in bone regeneration for tissue engineering. Biomol Eng 2007;24(6):613—8.
[33] Zhou L, Ogata Y. Transcriptional regulation of the human bone sialoprotein gene by fibroblast growth factor 2. J Oral Sci 2013;55(1):63—70.
[34] Joeng KS, Long F. Constitutive activation of Gli2 impairs bone formation in postnatal growing mice. PLoS One 2013;8(1):e55134.
[35] Kozhemyakina E, Lassar AB, Zelzer E. A pathway to bone: signaling molecules and transcription factors involved in chondrocyte development and maturation. Development 2015;142(5):817—31.
[36] Kalajzic I, Kalajzic Z, Kaliterna M, Gronowicz G, Clark SH, Lichtler AC, et al. Use of type I collagen green fluorescent protein transgenes to identify subpopulations of cells at different stages of the osteoblast lineage. J Bone Miner Res 2002;17(1):15—25.
[37] Yin D, Wang Z, Gao Q, Sundaresan R, Parrish C, Yang Q, et al. Determination of the fate and contribution of ex vivo expanded human bone marrow stem and progenitor cells for bone formation by 2.3ColGFP. Mol Ther 2009;17(11):1967—78.
[38] Ohba S, Ikeda T, Kugimiya F, Yano F, Lichtler AC, Nakamura K, et al. Identification of a potent combination of osteogenic genes for bone regeneration using embryonic stem (ES) cell-based sensor. FASEB J 2007;21(8):1777—87.
[39] Zujur D, Kanke K, Lichtler AC, Hojo H, Chung UI, Ohba S. Three-dimensional system enabling the maintenance and directed differentiation of pluripotent stem cells under defined conditions. Sci Adv 2017;3(5):e1602875.
[40] Buttery L, Bielby R, Howard D, Shakesheff K. Osteogenic differentiation of embryonic stem cells in 2D and 3D culture. Methods Mol Biol 2011;695:281—308.
[41] Caiazzo M, Okawa Y, Ranga A, Piersigilli A, Tabata Y, Lutolf MP. Defined three-dimensional microenvironments boost induction of pluripotency. Nat Mater 2016;15(3):344—52.
[42] Gadue P, Huber TL, Paddison PJ, Keller GM. Wnt and TGF-beta signaling are required for the induction of an in vitro model of primitive streak formation using embryonic stem cells. Proc Natl Acad Sci U S A 2006;103(45):16806—11.
[43] Sumi T, Tsuneyoshi N, Nakatsuji N, Suemori H. Defining early lineage specification of human embryonic stem cells by the orchestrated balance of canonical Wnt/beta-catenin, Activin/Nodal and BMP signaling. Development 2008;135(17):2969—79.
[44] Nizzardo M, Simone C, Falcone M, Locatelli F, Riboldi G, Comi GP, et al. Human motor neuron generation from embryonic stem cells and induced pluripotent stem cells. Cell Mol Life Sci 2010;67(22):3837—47.
[45] Komori T, Yagi H, Nomura S, Yamaguchi A, Sasaki K, Deguchi K, et al. Targeted disruption of Cbfa1 results in a complete lack of bone formation owing to maturational arrest of osteoblasts. Cell 1997;89(5):755—64.
[46] Nakashima K, Zhou X, Kunkel G, Zhang Z, Deng JM, Behringer RR, et al. The novel zinc finger-containing transcription factor osterix is required for osteoblast differentiation and bone formation. Cell 2002;108(1):17—29.
[47] Milona MA, Gough JE, Edgar AJ. Expression of alternatively spliced isoforms of human Sp7 in osteoblast-like cells. BMC Genomics 2003;4:43.
[48] Matsubara T, Kida K, Yamaguchi A, Hata K, Ichida F, Meguro H, et al. BMP2 regulates Osterix through Msx2 and Runx2 during osteoblast differentiation. J Biol Chem 2008;283(43):29119—25.
[49] Ulsamer A, Ortuno MJ, Ruiz S, Susperregui AR, Osses N, Rosa JL, et al. BMP-2 induces Osterix expression through up-regulation of Dlx5 and its phosphorylation by p38. J Biol Chem 2008;283(7):3816—26.
[50] Lu X, Gilbert L, He X, Rubin J, Nanes MS. Transcriptional regulation of the osterix (Osx, Sp7) promoter by tumor necrosis factor identifies disparate effects of mitogen-activated protein kinase and NF kappa B pathways. J Biol Chem 2006;281(10):6297—306.
[51] Maeda Y, Hojo H, Shimohata N, Choi S, Yamamoto K, Takato T, et al. Bone healing by sterilizable calcium phosphate tetrapods eluting osteogenic molecules. Biomaterials 2013;34(22):5530—7.
[52] Hurley MM, Abreu C, Harrison JR, Lichtler AC, Raisz LG, Kream BE. Basic fibroblast growth factor inhibits type I collagen gene expression in osteoblastic MC3T3-E1 cells. J Biol Chem 1993;268(8):5588—93.
[53] Rodan SB, Wesolowski G, Yoon K, Rodan GA. Opposing effects of fibroblast growth factor and pertussis toxin on alkaline phosphatase, osteopontin, osteocalcin, and type I collagen mRNA levels in ROS 17/2.8 cells. J Biol Chem 1989;264(33):19934—41.
[54] Naganawa T, Xiao L, Abogunde E, Sobue T, Kalajzic I, Sabbieti M, et al. In vivo and in vitro comparison of the effects of FGF-2 null and haplo-insufficiency on bone formation in mice. Biochem Biophys Res Commun 2006;339(2):490—8.
[55] Chen KG, Mallon BS, McKay RD, Robey PG. Human pluripotent stem cell culture: considerations for maintenance, expansion, and therapeutics. Cell Stem Cell 2014;14(1):13—26.
[56] Kawane T, Komori H, Liu W, Moriishi T, Miyazaki T, Mori M, et al. Dlx5 and Mef2 regulate a novel Runx2 enhancer for osteoblast-specific expression. J Bone Miner Res 2014;29(9):1960—9.
[57] Bruderer M, Richards RG, Alini M, Stoddart MJ. Role and regulation of RUNX2 in osteogenesis. Eur Cells Mater 2014;28:269—86.
[58] Dacic S, Kalajzic I, Visnjic D, Lichtler AC, Rowe DW. Col1a1-driven transgenic markers of osteoblast lineage progression. J Bone Miner Res 2001;16(7):1228—36.
[59] Sparks NRL, Martinez IKC, Soto CH, Zur Nieden NI. Low osteogenic yield in human pluripotent stem cells associates with differential neural crest promoter methylation. Stem Cells 2018;36(3):349—62.
[60] Hayashi K, Okamoto F, Hoshi S, Katashima T, Zujur DC, Li X, et al. Fast-forming hydrogel with ultralow polymeric content as an artificial vitreous body. Nat Biomed Eng 2017;1:44.